Nuclear Materials and Energy 12 (2017) 559–563

Contents lists available at ScienceDirect

Nuclear Materials and Energy

journal homepage: www.elsevier.com/locate/nme

Assessment of erosion, deposition and fuel retention in the JET-ILW divertor from ion beam analysis data

N. Catarino[a,b,*], N.P. Barradas[a,c], V. Corregidor[a,b], A. Widdowson[a,d], A. Baron-Wiechec[a,d], J.P. Coad[a,d], K. Heinola[a,e], M. Rubel[a,f], E. Alves[a,b], JET Contributors[1]

[a] EUROfusion Consortium, JET, Culham Science Centre, Abingdon OX14 3DB, UK
[b] IPFN, Instituto Superior Técnico, Universidade de Lisboa, Lisboa 1049-001, Portugal
[c] C²TN, Instituto Superior Técnico, Universidade de Lisboa, E.N. 10, Sacavém 2686-953, Portugal
[d] Culham Centre for Fusion Energy, Culham Science Centre, Abingdon OX14 3DB, UK
[e] University of Helsinki, P.O. Box 64, Helsinki 00560, Finland
[f] Royal Institute of Technology, Association EURATOM-VR, Stockholm SE-100 44, Sweden

ARTICLE INFO

Article history:
Received 14 July 2016
Revised 5 October 2016
Accepted 22 October 2016
Available online 18 November 2016

keywords:
JET
ITER-like wall
Plasma facing components
Erosion
Deposition
Ion beam analysis

ABSTRACT

Post-mortem analyses of individual components provide relevant information on plasma-surface interactions like tungsten erosion, beryllium deposition and plasma fuel retention with divertor tiles via implantation or co-deposition. Ion Beam techniques are ideal tools for such purposes and have been extensively used for post-mortem analyses of selected tiles from JET following each campaign.

In this contribution results from tiles removed from the JET ITER-Like Wall (JET-ILW) divertor following the 2013–2014 campaign are presented. The results summarize erosion, deposition and fuel retention along the poloidal cross section of the divertor surface and provide data for comparison with the first JET-ILW campaign, showing a similar pattern of material migration with the exception of Tile 6 where the strike point time on the tile was ~ 4 times longer in 2013–2014 than in 2011–2012, which is likely to account for more material migration to this region. The W deposition on top of the Mo marker coating of Tile 4 shows that the enrichment takes place at the strike point location.

1. Introduction

The future of fusion reactors will depend on the behaviour of the materials used in Plasma Facing Components (PFCs) which will determine their lifetime and also influence retention of hydrogen isotopes in the vessel. Among other processes, erosion of PFCs and subsequent re-deposition are critical for the operation of fusion devices and must be properly understood. The erosion and migration in the divertor is a complex system and determines the lifetime of PFCs in fusion devices. Erosion in the main chamber is the main source of impurities in the plasma, it occurs by sputtering of plasma ions with energies up to several keV and subsequent impact of eroded particles. The eroded material, mainly Be from the Be-coated tiles, enters the plasma, is ionised and transported by the SOL-flows towards the divertor during the X-point phase. This flow induces deposition of Be in the top part of the inner divertor. The process of re-erosion/deposition keeps going until it is deposited onto remote areas and no longer interacts with the plasma. The number of cycles of re-erosion/deposition decreases with the threshold energy of the element, this means that in remotes areas we expect more C than Be, and only a small amount of W [1]. The co-deposition of fuel particles with erosion products leads to an increase in the tritium inventory.

During the 2013–2014 JET-ILW campaign several marker tiles were installed in the main chamber and divertor to assess the global picture of erosion and re-deposition processes occurring during machine operation [2–4]. The divertor is the region where these processes are expected to occur at extreme conditions and post mortem analysis offers the possibility to reveal some of the major effects.

Fuel inventory, material erosion and melting have a major impact on the performance of the divertor. A large number of diagnostic tools have been used to study these phenomena. This study presents the results from Ion Beam Analysis (IBA) techniques such

* Corresponding address: IFPN/LATR, Instituto Superior Técnico (IST), Universidade de Lisboa, Estrada Nacional N° 10, km 139,7, Bobadela 2695-066, Portugal.
E-mail addresses: norberto.catarino@ctn.ist.utl.pt, norberto.catarino@ctn.tecnico.ulisboa.pt (N. Catarino).

[1] See the Appendix of F. Romanelli et al., Proceedings of the 25th IAEA Fusion Energy Conference 2014, Saint Petersburg, Russia

http://dx.doi.org/10.1016/j.nme.2016.10.027

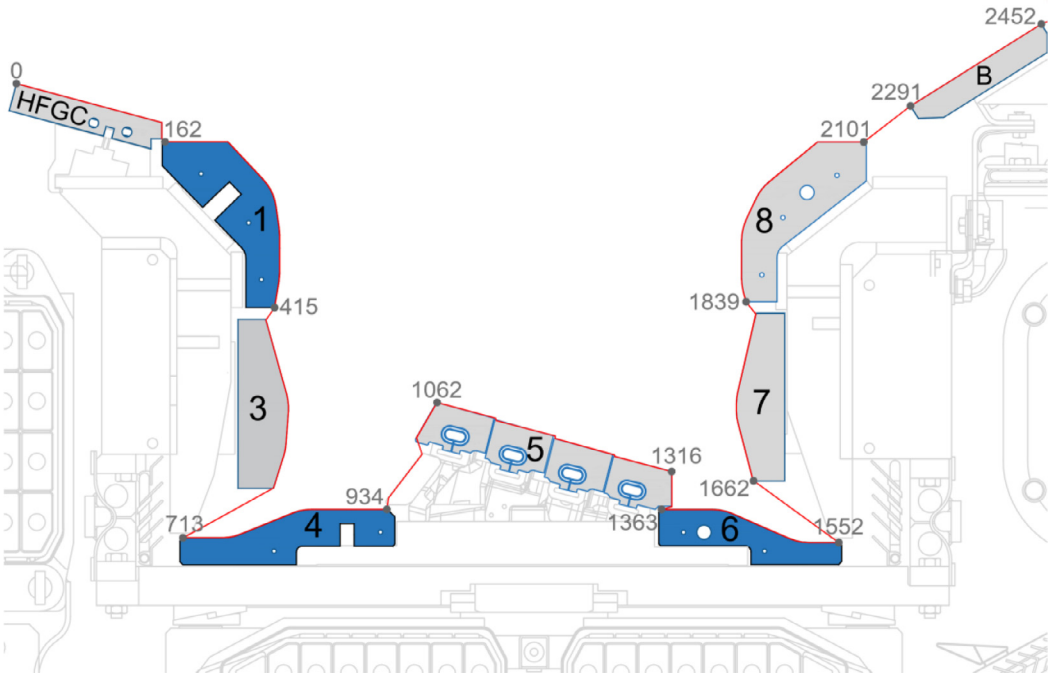

Fig. 1. JET divertor during the JET-ILW campaign 2013–2014. The s-coordinate (in mm) starts at the upper left corner of Tile 0 and follows the tile surfaces. In blue, the tiles studied in this paper; the Tile 1 is between s-coordinates 162 mm and 415 mm, Tile 4 between s-coordinates 713 mm and 934 mm and Tile 6 between s-coordinates 1363 mm and 1552 mm.

as Rutherford Backscattering Spectrometry (RBS) and Nuclear Reaction Analysis (NRA) for fuel retention and erosion patterns in JET. The results give information on the processes occurring at the inner and outer divertor corners as well as at the transition from the inner main chamber wall (high field side) to the inner divertor.

2. Experimental details

A selection of passive diagnostic components and marker tiles were installed in the JET chamber for the 2013–2014 campaign. The tile numbers and location in the divertor are shown in Fig. 1. In this work, results for divertor Tiles 1, 4 and 6, are presented, discussed and highlighted. The tiles are solid structures where the plasma facing surface is shaped with flat segments at different angles. This introduces some difficulties in mounting each tile for IBA which were overcome by measuring each of the flat segments separately, i.e. the tile was mounted in the chamber several times using specially designed holders to orient each surface perpendicular to the ion beam as shown in Fig. 2. All positions on divertor tiles are located using the s-coordinate system (Fig. 1), starting at the upper left corner of the High Field Gap Closure tile (Tile 0) and following the tile surfaces from the inner to the outer divertor.

The divertor tiles, with the exception of Tile 5, consist of CFC coated with 10 to 20 µm tungsten (W) on the plasma-facing surfaces [5,6]. Marker tiles, like Tile 1, used to study erosion and deposition in the divertor were coated with a W marker layer with a thickness of about 3 µm with a 3 µm thick molybdenum (Mo) interlayer between the W marker layer and the thick W coating [6]. The Mo interlayer is necessary to distinguish the W marker layer from the W coating for depth profiling methods, therefore enabling the erosion of W to be measured and the quantitative determination of deposition of all elements. The data presented for Tile 4 are from a marker tile where the top layer is 3 µm thick Mo (similar to Tile 1 but where the top W layer is omitted), which is used to enable the analysis of re-deposited W.

Erosion and deposition were analysed by Ion beam Analysis (IBA) techniques using the 2.5 MV Van de Graaff accelerator in-

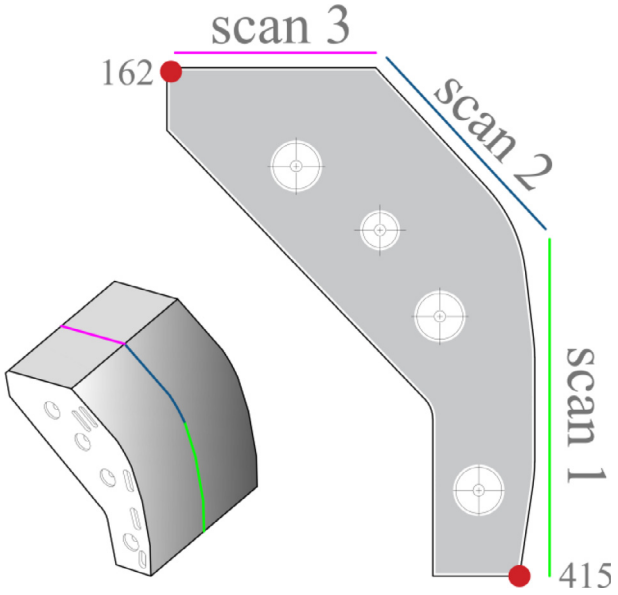

Fig. 2. Schematic view of a marker Tile 1. Due to the tile geometry three analysis scans were made as indicated in the diagram, in order to minimize the effect of the angle between the sample normal and the direction of the incident beam.

stalled at the Laboratory of Accelerators and Radiation Technologies of Instituto Superior Técnico. Analyses for JET were performed in a chamber dedicated to fusion research, where samples, including full JET tiles, contaminated with tritium (T) and beryllium (Be) can be handled.

Elastic Backscattering Spectrometry (EBS) and Particle Induced X-ray Emission (PIXE) were performed with 2.3 MeV incident protons. RBS and NRA were performed using ^{3}He ions at an energy of 2.3 MeV in order to measure the amounts of ^{2}H (D), Be and C. The D(^{3}He, p)^{4}He reaction was used to measure the D content, the ^{9}Be(^{3}He, p$_{x}$)^{11}B (x = 0,1,2,3) reactions [7] for Be and the

$^{12}C(^{3}He, p_0)^{14}N$ reaction for ^{12}C. For thin deposits, the NRA data provide more sensitive and accurate results for Be and C than the RBS data, which are used for thick deposits. At 2.3 MeV the NRA cross-section for carbon is very low, and in the case of thick films the signal from C ($^{12}C(^{3}He, p_0)^{14}N$) overlaps with the Be signal ($^{9}Be(^{3}He, p_3)^{11}B$), limiting its detection.

The sample manipulator in the experimental chamber is fully automated and enables analysis over 150 mm along the surface. This allows efficient measurement of whole JET tiles. The RBS particle detector is located at a scattering angle of 150° The NRA detector is placed at a 135° scattering angle and has an active layer with 1 mm thickness. A 140 µm thick Al stopping foil was selected to allow the detection of D and Be protons from the $^{2}H(^{3}He, p_0)^{4}He$ and $^{9}Be(^{3}He, p_x)^{11}B$ reactions [7] whilst stopping the 14 MeV α particles from the $^{9}Be(^{3}He, \alpha_0)^{8}Be$ reaction. Straggling in the foil does not affect the measurements since it is the signal integral that carries the information on the cross section. The X-rays are detected by PIXE by means of a "Sirius 30" detector located at a scattering angle of 150° with a Mylar filter 350 µm thick.

The tiles were scanned using EBS, RBS, NRA and PIXE, along the poloidal direction as indicated in Fig. 2 for Tile 1: spectra are taken every 5 mm using a 1 mm beam spot size along the tile surface to have a complete picture of the composition.

The experimental data were analysed using the NDF code [8] to quantify all the impurities present in the tiles. The sample composition is determined in a self-consistent way with PIXE data simulated by means of LibCPIXE code [9]. The PIXE data were analysed with GUPIX code [10] and the results used as input with NDF-LibCPIXE.

3. Results

The results are presented and discussed below for each of the tiles individually.

3.1. Upper inner divertor (Tile 1)

On the W surface Be deposits more than 10 µm thick were found at the top of Tile 1 in the region s = 162–296. In the first JET-ILW campaign this thick deposit was shown to be a layered structure, with varying Be and W concentrations probably due to operations history [11]. The non-uniform deposition and the surface roughness complicates the interpretation of layered structures by IBA, but the overall amount of deposited material is measured, e.g. the total areal densities of the chemical species. It should be pointed out that thick films tend to cause proton energy dispersion, not proton particle loss, and some dispersion can be tolerated; the 2.3 MeV incident protons have insufficient energy to resolve the thickness of the Be deposit without error. The EBS data together with PIXE and NRA give the concentration of the elements present in the layer. Depth profiles at each analysis point are integrated to give the concentration along the surface of Be, D, C and O in the first 5×10^{19} at/cm^2 of (~6 µm using the bulk densities and normalizing each density by the concentration of the corresponding element); over this integration depth the beam doesn't suffer large energy dispersion. These results are shown in Fig. 3. These thick deposits have a complex and multi-layer structure, showing a similar pattern to the first JET-ILW campaign [3]. The concentration of Be varies from 70% to 90%, D up to 6%, O and C from 1% to 10%. EBS proton spectra show W and Mo at the surface, but at concentrations below 1%.

In the lower part of Tile 1 (s = 296–415 mm) there is a small deposition of Be, D, C, and O, which is difficult to quantify. A similar pattern to the first JET-ILW campaign was observed [12]. This deposition is low due to competition between deposition and erosion processes occurring in this region.

3.2. Remote inner corner (Tile 4)

Deposits rich in D, Be, C and O as well as other metals are observed on Tile 4 in the plasma shadowed surface, i.e. the flat region of the tile below the slope (s = 713–762 mm), as shown in Fig. 3.During X-point plasmas neutrals erode Be from the inner wall. Eroded Be becomes ionised and is transported through the SOL [13] and is deposited in the divertor along with D and other impurities. On the plasma accessible surface of the tile deposited material is sputtered and redeposited until it migrates to the remote inner corner. This can be seen in Fig 3a where the Be thickness in the plasma accessible region (s > 775 mm, see Fig 3d) is nearly one order of magnitude lower than in the remote area (s < 775 mm). In addition the D content is also reduced in the plasma accessible surface due to heating of the surface [13], as shown in Fig 3b. The lower threshold energy of C and O compared with Be increases the number of cycles of erosion/deposition for these elements and extends their range giving higher concentrations in remote areas (see Fig 3c) compared with Be (Fig 3a).

At the predominant strike point position s = 798 mm the Mo marker layer is eroded by ~40% of the nominal thickness of 3 µm: the distribution of the strike points and the Mo concentration are shown in Fig. 4d and c respectively.

Having a Mo top surface allows W deposition to be measured. Three bands of W deposition in the toroidal direction are found as shown in Fig. 4b, one at the top of the sloping surface (s = 840 mm), a band at the predominant strike point position (s = 800 mm) and a band near the corner of the horizontal surface (s = 772 mm). Some erosion occurs on Tile 3 when the strike point is located there, as was observed after ILW-1 [12], and W eroded from this Tile may be transported by the SOL-flows towards Tile 4 in subsequent discharges to join W eroded locally from other (W-coated) Tile 4 when the strike point is located there. However, surface W is seen on all analysed surfaces in small quantities and generally in JET the most likely W source is erosion from the outer divertor tiles. Due to the higher threshold for re-erosion, W is enriched at the strike point location, where the flux and impact energy is insufficient for further migration into the shadowed zone: however Mo will be preferentially sputtered from this area as it has a lower sputtering threshold energy for re-erosion. The third band results probably from local re-deposition of the W on the tile. The rest of the tile (from s ≈ 840–934 mm), reveals a small amount of deposition, and no erosion. This deposition pattern is a little bit different than observed in the previous ILW campaign 2011–2012 [14] mainly because of changes in the strike point distribution between the campaigns.

3.3. Remote outer corner (Tile 6)

Deposition is also detected in the plasma shadowed outer corner of Tile 6, although ~5 times greater Be content than on Tile 4 and ~5 times higher than observed on Tile 6 after the 2011–2012 campaign [15]. The difference in the Be amount and profile [12] between both campaigns is due to an increase of the time of the outer strike point on Tile 6, that is ~4 times longer in 2013–2014 than in 2011–2012 as show in Fig 3d. On Tile 6 the deposition was inhomogeneous with deposition predominantly at the bottom of the sloping region in a band from s ≈ 1480 mm to s ≈ 1515 mm. Ni is observed in this deposit of the order of 2×10^{18} at/cm^2 likely due to some melting of Inconel tie rods in Tile 7.

In the plasma shadowed area of Tile 6 the D, C and O are present but at lower concentrations than observed in the plasma shadowed area of Tile 4, nevertheless the deposition mechanism in this zone should be the same. On the upper horizontal surface of the tile (s = 1363–1425 mm) the amount of D decreases an order to 1×10^{17} at/cm^2, the C and O are in the limit of the EBS/NRA

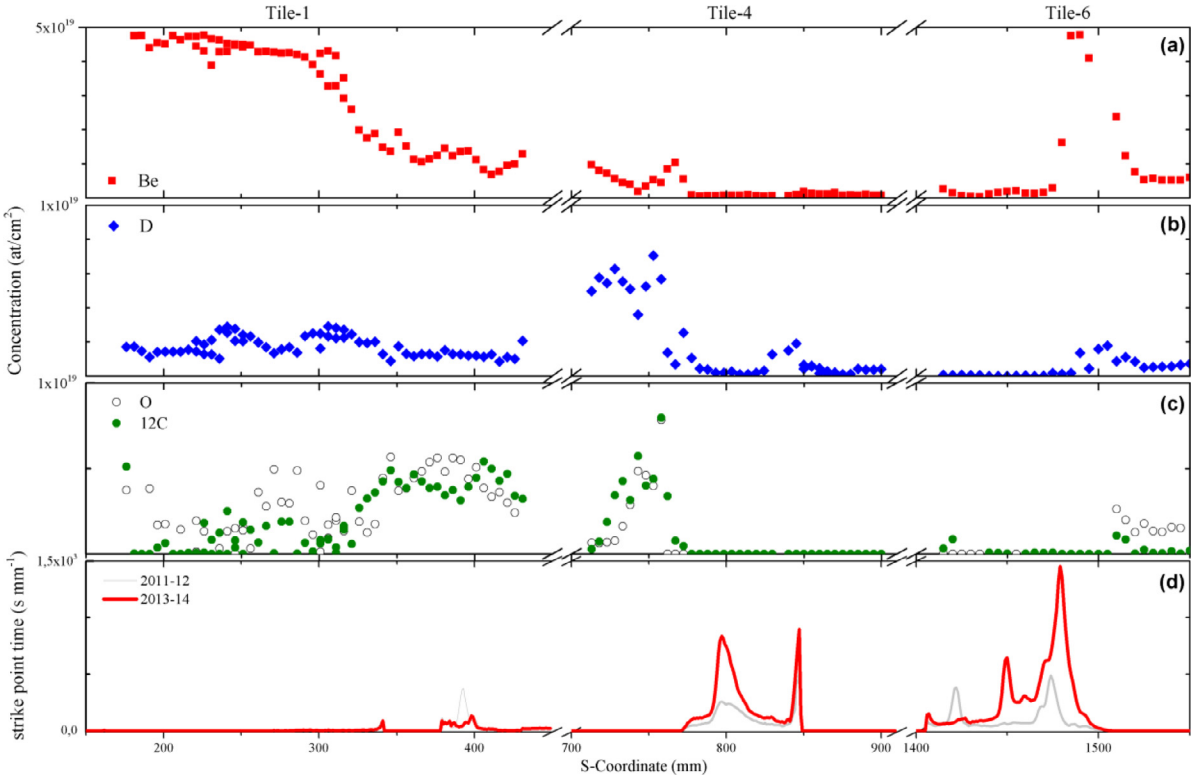

Fig. 3. Total deposition of (a) Be, (b) D, (c) C and O on the marker tiles. The concentration for Tile 1 is the integrated concentration in the first 5×10^{19} at/cm^2 of sample. (d) Strike point positions for the JET-ILW campaign 2011–12 and 2013–14.

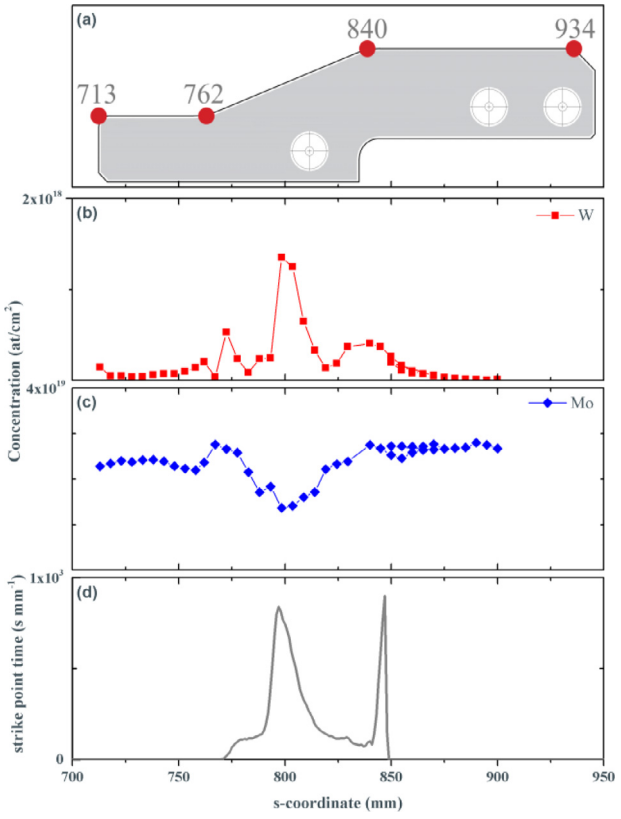

Fig. 4. Tile 4 (a) s-coordinate between 713 mm and 934, showing the regions referred to in the text. (b) Integration of W concentration in the first 10^{19} at/cm^2 of the tile surface (i.e. deposited on top of the marker) (c) Total concentration of the Mo marker layer, and (d) a histogram of strike point positions for the JET-ILW campaign 2013 to 2014.

sensitivity. This surface was partly shadowed by Tile 5 and was in the private flux region when the strike point was on tile 6. Tile 6 is a standard W coated tile, therefore it is not possible to comment where erosion occurred.

4. Conclusions

Under the present JET plasma conditions, the upper divertor remains the region of highest deposition with Be rich films over 10–20 µm thick present at the top of Tile 1. Fuel retention in the deposits on Tile 1 remain similar to the 2011–2012 campaign with Be: D ratio of the order (10–15):1, typically 5.0×10^{19} at/cm^2 of Be to 0.3×10^{19} at/cm^2 of D in the Be rich films.

Be and D in the remote inner corner of the divertor (Tile 4) are an order of magnitude higher ($\sim 5.0 \times 10^{18}$ at/cm^2 of D) than the maximum deposition seen beyond at the bottom of the sloping surface ($\sim 0.5 \times 10^{18}$ at/cm^2 of D), i.e., beyond s≈770 mm. Surface analysis of the Mo marker coating shows a W deposition in three locations: one at the predominant strike point position, one with the Be deposits and one at the top of the sloping surface.

Deposition at the outer corner of the divertor also shows a maximum deposition at the furthest region of the tile accessible by the plasma. The maximum Be deposited in this band is 3×10^{19} at/cm^2, around ~5 times higher than observed in the 2011–2012 campaign for similar total time in divertor X-point plasma - 13 h (2011–2012) compared with 14 h (2013–2014). However the time the outer strike point was located on Tile 6 was ~ 4 times longer in 2013–2014 than in 2011–2012, which is likely to account for more material migration to this region [16,15].

Acknowledgements

This work has been carried out within the framework of the EUROfusion Consortium and has received funding from the Eu-

ratom research and training programme 2014–2018 under grant agreement No 633053. The views and opinions expressed herein do not necessarily reflect those of the European Commission. This work was also part-funded by Portuguese FCT - Fundação para a Ciência e a Tecnologia, under grant PD/BD/52411/2013 (PD-F APPLAuSE) and through project Pest-OE/SADG/LA0010/2013.

Reference

[1] S. Brezinsek, J. Nucl. Mater. 463 (2015) 11–21.
[2] K. Heinola, A. Widdowson, J. Likonen, E. Alves, A. Baron-Wiechec, N.P. Barradas, S. Brezinsek, N. Catarino, J.P. Coad, S. Koivuranta, S. Krat, G.F. Matthews, M. Mayer, P. Petersson, J.-E. Contributors, Phys. Scr. T167 (2016) 14075.
[3] A. Baron-Wiechec, A. Widdowson, E. Alves, C.F. Ayres, N.P. Barradas, S. Brezinsek, J.P. Coad, N. Catarino, K. Heinola, J. Likonen, G.F. Matthews, M. Mayer, P. Petersson, M. Rubel, W. van Renterghem, I. Uytdenhouwen, J. Nucl. Mater. 463 (2015) 157–161.
[4] A. Widdowson, E. Alves, C.F. Ayres, A. Baron-Wiechec, S. Brezinsek, N. Catarino, J.P. Coad, K. Heinola, J. Likonen, G.F. Matthews, M. Mayer, M. Rubel, Phys. Scr. T159 (2014) 14010.
[5] M. Rubel, J.P. Coad, A. Widdowson, G.F. Matthews, H.G. Esser, T. Hirai, J. Likonen, J. Linke, C.P. Lungu, M. Mayer, L. Pedrick, C. Ruset, J. Nucl. Mater 438 (2013) S1204–S1207.
[6] C. Ruset, E. Grigore, I. Munteanu, H. Maier, H. Greuner, C. Hopf, V. Phylipps, G.F. Matthews, Fusion Eng. Des. 84 (2009) 1662–1665.
[7] N.P. Barradas, N. Catarino, R. Mateus, S. Magalhães, E. Alves, Z. Siketić, I.B. Radović, Nucl. Instruments Methods Phys. Res. Sect. B Beam Interact. Mater. Atoms 346 (2015) 21–25.
[8] N.P. Barradas, C. Jeynes, Nucl. Instruments Methods Phys. Res. Sect. B Beam Interact. Mater. Atoms 266 (2008) 1875–1879.
[9] C. Pascual-Izarra, N.P. Barradas, M.A. Reis, Nucl. Instruments Methods Phys. Res. Sect. B Beam Interact. Mater. Atoms 249 (2006) 820–822.
[10] J.A. Maxwell, W.J. Teesdale, J.L. Campbell, Nucl. Instruments Methods Phys. Res. Sect. B Beam Interact. Mater. Atoms 95 (1995) 407–421.
[11] H. Bergsåker, I. Bykov, Y. Zhou, P. Petersson, G. Possnert, J. Likonen, J. Petterson, S. Koivuranta, A. Widdowson, Phys. Scr. T167 (2016) 14061.
[12] M. Mayer, S. Krat, W. Van Renterghem, A. Baron-Wiechec, S. Brezinsek, I. Bykov, J.P. Coad, Y. Gasparyan, K. Heinola, J. Likonen, A. Pisarev, C. Ruset, G. de Saint-Aubin, A. Widdowson, Phys. Scr. T167 (2016) 14051.
[13] K. Sugiyama, C. Porosnicu, W. Jacob, I. Jepu, C.P. Lungu, Nucl. Mater. Energy 6 (2016) 1–9.
[14] K. Heinola, A. Widdowson, J. Likonen, E. Alves, A. Baron-Wiechec, N.P. Barradas, S. Brezinsek, N. Catarino, J.P. Coad, S. Koivuranta, G.F. Matthews, M. Mayer, P. Petersson, J. Nucl. Mater. 463 (2015) 961–965.
[15] P. Petersson, M. Rubel, H.G. Esser, J. Likonen, S. Koivuranta, A. Widdowson, J. Nucl. Mater. 463 (2015) 814–817.
[16] A. Widdowson, E. Alves, A. Baron-Wiechec, N.P. Barradas, N. Catarino, J.P. Coad, V. Corregidor, A. Garcia-Carrasco, K. Heinola, S. Koivuranta, S. Krat, A. Lahtinen, J. Likonen, M. Mayer, P. Petersson, S. van Boxel, Nucl. Mater. Energy (n.d.) These Proceedings (2016).